Stasiunas, Rytis; Miah, Md Suzan; Heino, Mikko; Haneda, Katsuyuki; Icheln, Clemens

Real-Time Demonstration of Antenna Effects on Emulated Wireless Capsule Endoscope Links

Published in:
14th European Conference on Antennas and Propagation, EuCAP 2020

DOI:
10.23919/EuCAP48036.2020.9135599

Published: 01/03/2020

Document Version
Peer reviewed version

Please cite the original version:
Stasiunas, R., Miah, M. S., Heino, M., Haneda, K., & Icheln, C. (2020). Real-Time Demonstration of Antenna Effects on Emulated Wireless Capsule Endoscope Links. In *14th European Conference on Antennas and Propagation, EuCAP 2020* Article 9135599 (Proceedings of the European Conference on Antennas and Propagation). IEEE. https://doi.org/10.23919/EuCAP48036.2020.9135599

Real-Time Demonstration of Antenna Effects on Emulated Wireless Capsule Endoscope Links

Rytis Stasiunas, Pasi Koivumäki, Md. Suzan Miah, Mikko Heino, Katsuyuki Haneda and Clemens Icheln
Aalto University School of Electrical Engineering, Espoo, Finland E-mail: pasi.koivumaki@aalto.fi

***Abstract*—A real-time over-the-air video transfer platform is developed for a wireless capsule endoscope scenario. With this platform, we aim at providing an intuitive and instant understanding of antenna effects on both quantitative and qualitative radio link performance, e.g., on video image quality, on bit error rate (BER) and on constellation diagrams of digital modulation. The platform consists of a host computer and a universal software-defined peripheral, complemented with an endoscope capsule mockup that includes an antenna, on-body antenna, and a liquid body phantom for creating a realistic inbody-to-onbody radio link scenario. The antennas operate at 433 MHz, while the liquid mimics the complex permittivity of colon tissue at that frequency range. Uncoded orthogonal frequency division multiplexing with 2.3 MHz bandwidth is adopted as a physical layer. Footage of the real-time demonstration is available from the link in [1] and shows the clear effects on radio link performance when 1) the distance of the capsule antenna from the wall of the liquid phantom is increased, and 2) when capsule antenna is moved out of the liquid phantom. In both cases, disruption of the video images is observed, due to an increased BER. The BER plots are reproduced in this paper as evidence. The demonstration has been used for post-graduate education to deepen students' understanding of the importance of antenna design, while the same benefit may be expected when showing the video to clinical experts who operate capsule endoscopes.**

I. Introduction

Endoscopy is a popular technology in the diagnosis and treatment of the digestive tract. The wireless capsule endoscope is the most recent variant of the technology, which was first discussed in 2000 [2]. Patients swallow the wireless endoscopy capsule, which is similar in size as a vitamin pill. The capsule contains various electronic components for the endoscopic operation. An embedded camera takes video images inside the digestive tract, and in case of wireless capsule endoscopy, the capsule sends images to outside the body for recording and inspection by physicians. Capsule endoscopy is particularly advantageous for inspecting the small intestine which is the part of the digestive tract hardest to reach e.g. when trying to find pathological tissues, e.g., cancer, among others [3]. Diagnosis and therapy with the capsule are minimally invasive and have a low-risk of infection and complication and hence this procedure is preferable by patients. Furthermore, capsule endoscopy allows more cost-effective diagnostics because it can be operated with a smaller number of physicians. Diagnostic indications found with the capsule endoscope are of great use for further tests by other endoscopy techniques [4]. Despite the wide-spread use of wireless capsule endoscope, there is still a need for improving its diagnostic yield by means of improved electronics and wireless communications. The latter is necessary for supporting video transfer of a higher number of pixels and frames per second by implementing new antennas and optimizing physical layer schemes. Experimental studies covering such aspects are, e.g., [5]–[8]. Real-time demonstration of video transmission over wireless capsule endoscope links is an effective means for presenting the effects of more advanced electronics as reported in [6], [7], especially for clinical experts who are involved in the development of improved capsule endoscope but are not necessarily familiar with electronics and wireless communications. The same is true for demonstrating the relevance of better antenna designs with respect to the link performance. For that purpose, we develop a real-time video transmission platform. The platform consists of capsule and on-body antennas operating at 433 MHz and a liquid phantom emulating electrical parameters of colon tissue; they are presented in the authors' earlier work [8]. In addition, we introduce a universal software-defined radio peripheral (USRP) to realise the real-time video transfer. The two major problems that we address in this paper are

- *a very limited availability of real-time demonstration platforms of wireless data transfer* in capsule endoscope scenarios to show the effect that antennas have on the link performance; in contrast, computing the theoretical capacity or bit error rate (BER) based on communication theory is not the most attractive way to demonstrate the same, especially to non-experts; and
- *non-existent experimental evidence* for the significance of better antenna designs and their effect on the radio link performance, i.e., on BER and throughput, in the capsule endoscope scenarios.

The main contributions of this work are

- *the development of a USRP-based real-time platform for transferring video images over an in-body to on-body radio link* in a capsule endoscope scenario.
- *real-time demonstration of the effects that the in-body capsule antenna* has on the link performance, utilizing the developed video transfer platform.

The remainder of this paper is organized as follows. Section II describes the implementation of the video transfer platform, exploiting both a host computer and a finite programmable gate array (FPGA) on board the USRP. The antennas and the body phantoms used in the demo are also introduced. Section III discusses antenna effects on the link quality of the wireless capsule endoscope link both through

TABLE I
TRANSCEIVER INITIALIZATION PARAMETERS AND THEIR VALUES

Parameter	Transmitter	Receiver
Frequency	433 MHz	433 MHz
Output power	0 dBm	Not applicable
Reference level	Not applicable	−10 dBm
Sample rate	2.5 MS/s	2.5 MS/s
Start trigger	Immediate	Immediate
Generation mode	Continuous	Continuous

quantitative and qualitative metrics; the realized footage of the video transfer using the platform is available online [1]. The paper is concluded in Section IV.

II. VIDEO TRANSFER PLATFORM FOR A CAPSULE ENDOSCOPE SCENARIO

In this section, we describe the control software and the setup of the over-the-air real-time video transfer platform that emulates the capsule endoscope scenario. It consists of a host laptop computer, a USRP, and the capsule and on-body antennas installed in and on a liquid body phantom, respectively. The control software running on the host computer obtains video data from a user datagram protocol (UDP) port on the same computer, and transmits it to the input buffer of the USRP transmitter (Tx). At the same time, the control software forwards the video data received from the USRP receiver (Rx) to another UDP port on the computer. The USRP continuously transmits and receives the video data through an orthogonal frequency division multiplexing (OFDM) waveform with a bandwidth of 2.3 MHz. The modulation and demodulation is implemented on the integrated FPGA board of the USRP. Two parallel instances of the VLC media player carry out the video streaming to one UDP port, and the decoding from the second UDP port, respectively. Details are described in the following.

A. Transmitter Configuration and Task Separation

The full functionality of the video transfer platform could only be achieved distributing the necessary tasks between the host computer and the FPGA board inside the USRP. This allows us to utilize the high speed of the FPGA board for the computationally heavy data processing, i.e., OFDM modulation and demodulation, while the host computer manages the non-constant data rate of the video hereby ensuring that the USRP transmits and receives at a constant data rate.

1) Host Computer Tx: The main tasks of the host computer are to initialize the control software implemented in LabView, to receive the video data from the UDP port, to send the transmission frames containing both video and random data to the USRP Tx. The use of random data makes sure that the transmission frames are sent at a constant data rate and no buffer underflow occurs. The initialization of the control software requires various constant values to be defined for the transmit and receive operations of the USRP, as exemplified in Table I for the case of this capsule endoscope scenario.

After initializing the control software, we create a random byte array, i.e., a transmission frame composed of 4700 unsigned 8-bit (U8) elements (bytes). The frame length was chosen to enable inserting the video data, which come as a U8 array of 2820 bytes, that is to be transmitted by the USRP. The preparation of the transmission frames in Labview happens in two independent `while`-loops. One of the loops receives video data from the UDP port and queues them in a first-input first-output (FIFO) buffer. While the other loop inserts the video data from the queue into transmission frames and forwards them to the FPGA module of the USRP for further processing through the direct memory access (DMA) buffer. A block diagram of the Tx control software implemented in the host computer can be seen in the top-left box of Fig. 1.

2) USRP FPGA Tx: The video data encapsulated into transmission frames need to be modulated in the USRP Tx, so that they can be sent over-the-air. OFDM modulation can be implemented on the FPGA board of the USRP, thanks to its sufficient clock speed. The transmission frames are split into arrays of 94 bytes. They are mapped into complex amplitudes at baseband, i.e., symbols, according to quadrature phase-shift keying (QPSK) mapping. After every fourth data symbol, a reference symbol is inserted for channel estimation and BER calculation, leading to an array with 470 data subcarriers. Furthermore, 21 null subcarriers are inserted at the lowest and highest sides of the band so that a 512-point inverse fast-Fourier transformation (IFFT) can be applied to this array. Finally, we add a cyclic prefix (CP) of $N_{\mathrm{CP}} = 128$ samples in the time domain, ending up with $N_{\mathrm{S}} = 640$ samples of a single OFDM frame ready to be transmitted. The operation of OFDM modulation inside the FPGA can be seen in Fig. 1 in the top-right box.

B. Receiver Configuration and Task Separation

As for the Tx, also the Rx takes advantage of the high speed of the FPGA in the USRP for the demodulation operation, so that finally the computational load for the host computer is small. The host computer performs QPSK symbol equalization and de-mapping, followed by video data extraction from the recovered transmission frames. The video frames are delivered to the UDP port and can then be viewed in the VLC video player. The required constant values during initialization of the Rx are found in Table I, where the Reference Level of the Rx denotes the dynamic range of the received signals.

1) USRP FPGA Rx: After the radio signals are received by the on-body antenna and sampled in the USRP, it is necessary to find the beginning of each OFDM frame to be able to properly demodulate it. For that, we use the Van de Beek algorithm [9]. This algorithm gives a maximum likelihood estimation of the symbol time and frequency offset by utilizing the correlation properties of the cyclic prefix; 640 time-samples following the start time index are processed for demodulation after removing the CP, performing a Fast-Fourier transformation (FFT), removing the null subcarriers and separating the data symbols from the reference symbols. The radio channel is estimated by comparing the complex amplitudes of the transmitted and acquired reference symbols. Even though the reference symbols are scattered only to a

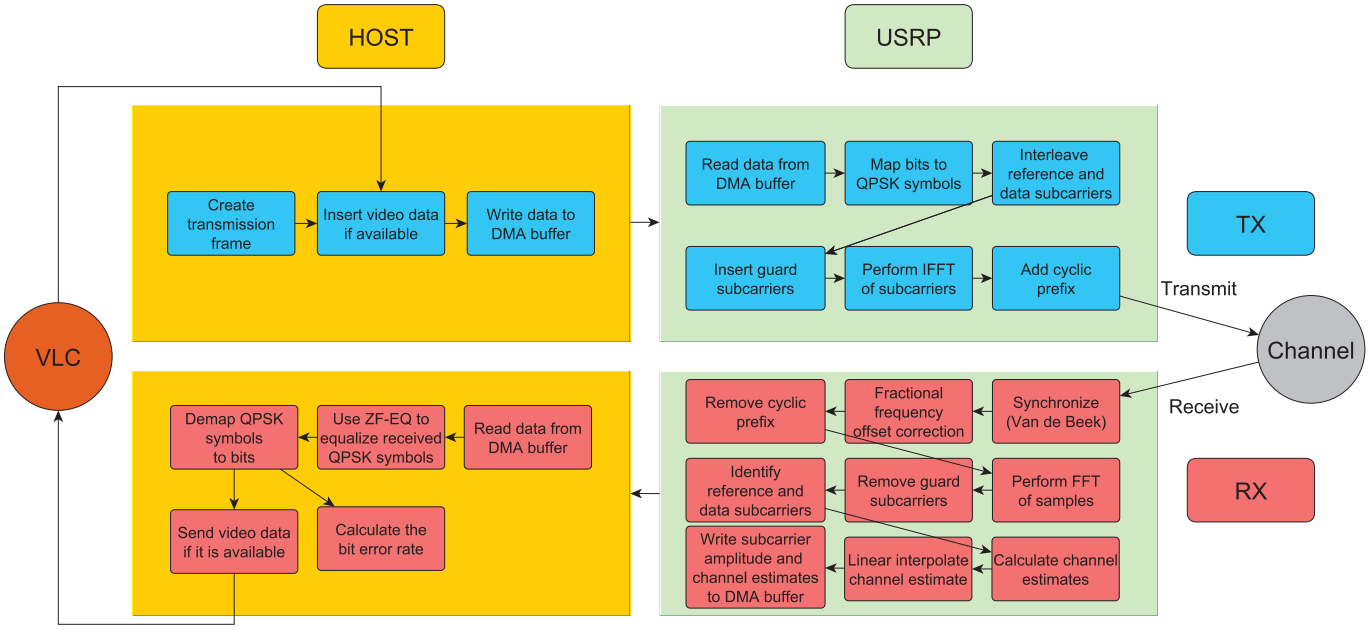

Fig. 1. High-level block diagram of the system.

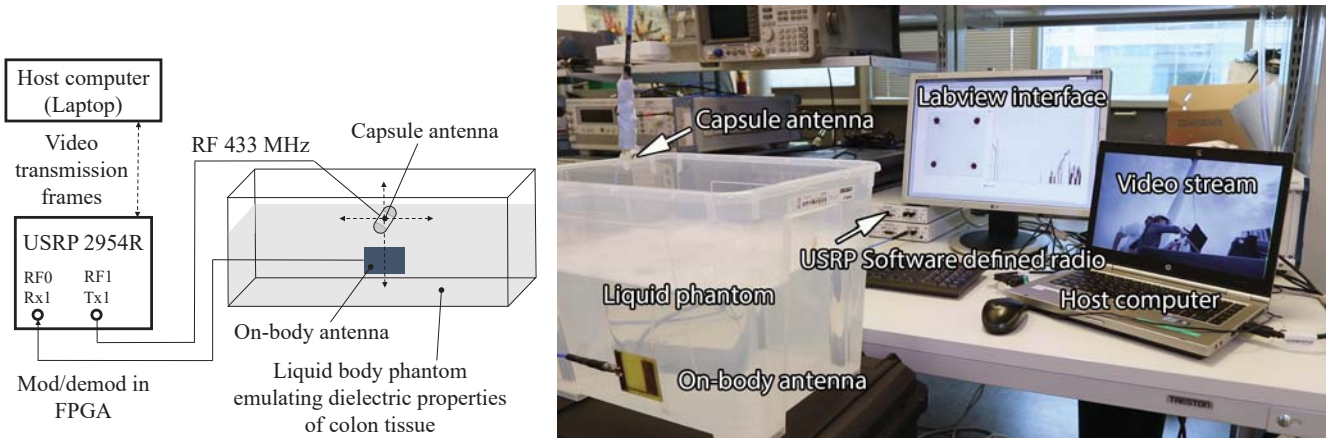

Fig. 2. (a) Block diagram and (b) physical realization of the real-time video transmission platform for capsule endoscope scenarios. In (a), the dotted double-arrow lines appended to the capsule antenna show two trajectories of capsule movement for observation of video images and link quality detailed in Section III.

few subcarriers, it is possible to obtain a channel estimate across all subcarriers through an implicit linear interpolation of the FFT, i.e. through interleaving the reference and data subcarriers. The operation of the OFDM demodulation inside the FPGA can be seen in Fig. 1 in bottom-right box.

2) Host Computer Rx: The host computer receives two arrays of data from the USRP Rx through two FIFO buffers. Firstly, an interpolated channel estimate across subcarriers, and secondly the transmission frames consisting of un-equalized complex amplitudes of QPSK symbols. Zero-forcing is applied to equalize the symbols for QPSK de-mapping, and then the transmission frames are recovered in the form of bytes. Random byte arrays that have nothing to do with the video data are removed from the recovered transmission frame. Finally, recovered video data is made available to the VLC video player through the UDP port. BER is calculated using the recovered random byte arrays. A block diagram of the Rx control software implemented in the host computer can be seen in the bottom-left box in Fig. 1.

C. Setup of the Demonstration

In this work, the capsule endoscope scenario is emulated using capsule and on-body antennas, along with a liquid human-body phantom. A block diagram and physical setup of the demonstration is illustrated in Fig. 2, integrating the host computer, the USRP, antennas and the body phantom.

(a) (b)

Fig. 3. (a) Transmit capsule antenna and (b) receive on-body monopole antenna operating at 433 MHz; design details are in [8].

In this subsection, we summarize the main characteristics of the antennas and the phantom based on experiments. For more design details and an experimental verification of the antennas and phantom, see [8].

1) Body Phantom: A cuboid-shaped plastic container is filled with a colon-mimicking liquid forming the phantom. The liquid was formulated by mixing 79 % salted water and 21 % TritonX-100. The mixing process consists of dissolving the salt in distilled water as 7.85 g/L, and then separately heating the TritonX-100 and salted water to 40 C° before mixing them. We used an HP 8720C network analyzer and an HP 85070A dielectric probe kit [10] based on the transmission line propagation method to verify the electrical properties of the liquid. The measured permittivity and loss tangent values at 433 MHz were $\epsilon_{\rm r} = 61.4$ and $\tan\delta = 0.60$, respectively, sufficiently close to the expected dielectric properties of the colon tissue $\epsilon_{\rm r} = 62.4$ and $\tan\delta = 0.58$.

2) Capsule Antenna: The capsule antenna is illustrated in Fig. 3(a). It is a loop antenna attached on the outer surface of a standard capsule. The antenna element was first printed on a flexible substrate material and then wrapped around the outer-wall of an empty capsule module to form a loop. The capsule module is made of polystyrene with $\epsilon_{\rm r} = 2.6$ and $\tan\delta = 0.05$ at 1 GHz. The diameter and length of the capsule are 11 and 27 mm, respectively, whereas the thickness of the capsule wall is 0.5 mm. Since the proposed loop antenna is a balanced structure in terms of current flow, a wideband, surface-mount balun is integrated to feed the radio signals conveniently, using an unbalanced coaxial cable and an SMA connector. During the demonstration, we used a layer of sticky rubber with $\epsilon_{\rm r} = 2.2$, $\tan\delta = 5.0 \times 10^{-4}$ around the feeding components, i.e., balun, SMA connector and coaxial cable, to avoid their direct contact with the liquid. When the capsule is at the center of the body phantom, the reflection coefficient of the capsule antenna is smaller than -10 dB over a 770 MHz bandwidth, including the operating radio frequency of our demonstration at 433 MHz.

3) On-Body Antenna: The on-body antenna is printed on a 1.5 mm thick FR4 substrate with $\epsilon_{\rm r} = 4.3$ as depicted in Fig. 3(b). A meandered monopole with a loaded patch is seen as the radiating element on the front side, while the ground plane is patterned on the other side of the substrate. The metallization layers are 19μmthick copper. A measurement of antenna matching, where the antenna was placed on the outer wall of the liquid container, shows that it resonates at 420 MHz with a -10 dB impedance bandwidth of 120 MHz.

III. Results and Discussions

A. Two Trajectories of Capsule Antenna's Movement

The platform in Fig. 2 was used to demonstrate real-time video transfer for varying locations of the capsule antennas, along with qualitative and quantitative link performance estimation such as BER and a plot of constellation pattern. Two types of trajectories of the capsule were tested, i.e., 1) the capsule moves from the nearest point of the on-body antenna in the liquid phantom to furthest point in the phantom and back, repeated twice and 2) the capsule is lifted out of the liquid phantom into free space and back again. The two trajectories are illustrated in Fig. 2(a) and referred to as "near-to-far test" and "body-to-air test" hereinafter, respectively. During the demonstration, some scattering may exist from a metallic instrument surrounding the platform, but the transmit power was set low enough (see Table I) so that only the strongest direct coupling between the capsule and on-body antennas dominates the radio channel characteristics. Frequency selective fading was not observed in the channel estimates over OFDM subcarriers spanning 2.3 MHz bandwidth.

B. Near-to-Far Test

Figure 4 shows measured BER during the two trajectories of capsule movement inside/outside the body phantom. The time-index on the x-axes corresponds 78.125 ms, adding up to 62.5 s across the shown 800 time-indices. The near-to-far test shows that the BER is very high when the capsule is very far from the on-body antenna due to insufficient signal-to-noise ratio (SNR) at the receiver. The quality of the video images deteriorates clearly with decreasing SNR. It must be noted that the Rx noise level is intentionally set higher than usual in this demonstration by adjusting the Rx reference level, shown in Table I, so that the link quality and hence the video quality degrades visually, while the capsule antenna is far away from the on-body antenna. Setting a lower Rx reference level, which is a more usual choice, would allow error-free video transfer across the liquid phantom, which is accordingly to the link budget analysis of our demonstration setup previously reported in [8].

C. Body-to-Air Test

The body-to-air test shows high BER when the capsule antenna moves out of the liquid due to two possible effects, i.e., 1) de-tuning of the capsule antenna when it operates in free-space and 2) increasing distance between the antennas. Again, it must be noted that the Rx noise level is set such that combination of these effects leads to degradation of SNR and hence increased BER. As the capsule antenna is designed to radiate properly in various organs of the digestive

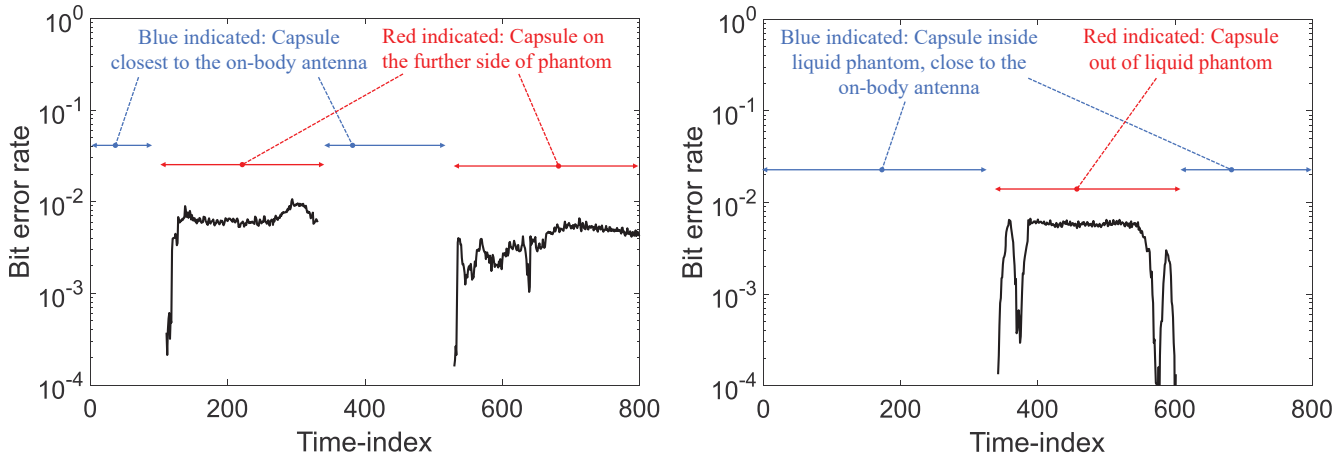

Fig. 4. Bit error rate over time for two types of capsule trajectories: (a) the capsule moves from closest to furthest points in the liquid phantom and back, repeated twice, i.e., near-to-far test; (b) the capsule goes out of the liquid phantom to free space and back, i.e., body-to-air test. The two trajectories are illustrated in Fig. 2(a). A time-index on the x axes corresponds 78.125 ms, making the mentioned 800 time-indices equivalent to 62.5 s.

tract, e.g., colon, small intestine and stomach which have $\epsilon_r > 50$, bringing the antenna to the air strongly affects the designed impedance matching. The video image quality drops completely when the capsule antenna is in the air. This nicely visualizes the impact of antenna de-tuning on the link quality.

D. Footage of Video Transfer Tests

The recorded footage of the video transfer demonstration, including both the near-to-far and body-to-air tests, is available online at [1].

IV. Concluding Remarks

In this paper, we elaborated the implementation of a real-time over-the-air video transfer platform for capsule endoscope scenarios. The platform aims at facilitating intuitive and instant understanding of antenna effects on the link quality, particularly targeting those who are involved with the development of improved wireless capsule endoscope but are not necessarily familiar with electronics and wireless communications. For the same purpose, the platform has also been used in graduate and post-graduate courses covering antennas, radio propagation and wireless systems. The platform consists of a USRP, capsule and on-body antennas operating at 433 MHz, and a liquid phantom emulating electrical parameters of the colon tissue at that frequency range. The entire functionality of the video data transfer is implemented in the host computer and the FPGA on the USRP, where uncoded OFDM with 2.3 MHz bandwidth was adopted. Real-time over-the-air video transfer was successfully demonstrated, where the effects of antenna detuning and link distance between the capsule and on-body antennas clearly reflect into the received video quality [1], constellation patterns and bit error rates.

References

[1] R. Stasiunas, M. Heino, C. Icheln, and K. Haneda, "Demo of wireless HD-video transfer from inside a human-body-phantom to an on-body receiver," https://research.aalto.fi/en/datasets/demo-of-wireless-hdvideo-transfer-from-inside-a-humanbodyphantom-to-an-onbody-receiver(e0cf3b6b-edd3-4e85-849f-caf19c9749b9).html.

[2] G. Iddan, G. Meron, A. Glukhovsky, and P. Swain, "Wireless capsule endoscopy," *Nature*, vol. 405, no. 6785, p. 417, May 2000.

[3] A. Koulaouzidis, E. Rondonotti, and A. Karargyris, "Small-bowel capsule endoscopy: a ten-point contemporary review," *World J Gastroenterol*, vol. 19, no. 24, p. 3726–3746, June 2013.

[4] G. Gay, M. Delvaux, and I. Fassler, "Outcome of capsule endoscopy in determining indication and route for push-and-pull enteroscopy," *Endoscopy*, vol. 38, no. 1, pp. 49–58, Jan. 2006.

[5] Q. Wang, K. Wolf, and D. Plettemeier, "An UWB capsule endoscope antenna design for biomedical communications," in *Proc. 2010 3rd Int. Symp. Applied Sci. Biomedical and Commun. Tech. (ISABEL 2010)*, Rome, Italy, Nov. 2010, pp. 1–6.

[6] Y. Gao, Y. Zheng, S. Diao, W. Toh, C. Ang, M. Je, and C. Heng, "Low-power ultrawideband wireless telemetry transceiver for medical sensor applications," *IEEE Trans. Biomedical Eng.*, vol. 58, no. 3, pp. 768–772, Mar. 2011.

[7] K. M. S. Thotahewa, J. Redoute, and M. R. Yuce, "Electromagnetic power absorption of the human abdomen from IR-UWB based wireless capsule endoscopy devices," in *Proc. 2013 IEEE Int. Conf. Ultra-Wideband (ICUWB 2013)*, Sydney, Australia, Sep. 2013, pp. 79–84.

[8] M. Suzan Miah, A. N. Khan, C. Icheln, K. Haneda, and K. Takizawa, "Antenna system design for improved wireless capsule endoscope links at 433 MHz," *IEEE Trans. Ant. Prop.*, vol. 67, no. 4, pp. 2687–2699, Apr. 2019.

[9] J. J. van de Beek, M. Sandell, and P. O. Borjesson, "ML estimation of time and frequency offset in OFDM systems," *IEEE Trans. Signal Processing*, vol. 45, no. 7, pp. 1800–1805, July 1997.

[10] M. M. Suzan, K. Haneda, C. Icheln, A. Khatun, and K. Takizawa, "An ultrawideband conformal loop antenna for ingestible capsule endoscope system," in *2016 10th European Conf. Ant. Prop. (EuCAP 2016)*, Davos, Swizterland, Apr. 2016, pp. 1–5.